UC Berkeley

UC Berkeley Previously Published Works

Title

Influence of Nonuniform Micron-Scale Strain Distributions on the Electrical Reorientation of Magnetic Microstructures in a Composite Multiferroic Heterostructure

Permalink

https://escholarship.org/uc/item/5s6227r8

Journal

Nano Letters, 18(3)

ISSN

1530-6984

Authors

Conte, Roberto Lo
Xiao, Zhuyun
Chen, Cai
et al.

Publication Date

2018-03-14

DOI

10.1021/acs.nanolett.7b05342

Peer reviewed

eScholarship.org Powered by the California Digital Library
University of California

NANO LETTERS
Cite This: Nano Lett. 2018, 18, 1952−1961
Letter
pubs.acs.org/NanoLett

Influence of Nonuniform Micron-Scale Strain Distributions on the Electrical Reorientation of Magnetic Microstructures in a Composite Multiferroic Heterostructure

Roberto Lo Conte,*[,†] Zhuyun Xiao,[‡] Cai Chen,[§] Camelia V. Stan,[∥] Jon Gorchon,[†,⊥] Amal El-Ghazaly,[†] Mark E. Nowakowski,[†] Hyunmin Sohn,[‡] Akshay Pattabi,[†] Andreas Scholl,[∥] Nobumichi Tamura,[∥] Abdon Sepulveda,[§] Gregory P. Carman,[§] Robert N. Candler,[‡,§,#] and Jeffrey Bokor*[,†,⊥]

[†]Department of Electrical Engineering and Computer Science, University of California, Berkeley, California 94720, United States
[‡]Department of Electrical Engineering, University of California, Los Angeles, California 90095, United States
[§]Department of Mechanical and Aerospace Engineering, University of California, Los Angeles, California 90095, United States
[∥]Advanced Light Source, Lawrence Berkeley National Lab, Berkeley, California 94720, United States
[⊥]Materials Sciences Division, Lawrence Berkeley National Laboratory, Berkeley, California 94720, United States
[#]California NanoSystems Institute, Los Angeles, California 90095, United States

Supporting Information

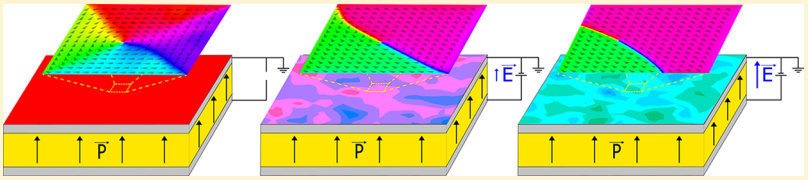

ABSTRACT: Composite multiferroic systems, consisting of a piezoelectric substrate coupled with a ferromagnetic thin film, are of great interest from a technological point of view because they offer a path toward the development of ultralow power magnetoelectric devices. The key aspect of those systems is the possibility to control magnetization via an electric field, relying on the magneto-elastic coupling at the interface between the piezoelectric and the ferromagnetic components. Accordingly, a direct measurement of both the electrically induced magnetic behavior and of the piezo-strain driving such behavior is crucial for better understanding and further developing these materials systems. In this work, we measure and characterize the micron-scale strain and magnetic response, as a function of an applied electric field, in a composite multiferroic system composed of 1 and 2 μm squares of Ni fabricated on a prepoled $[Pb(Mg_{1/3}Nb_{2/3})O_3]_{0.69}-[PbTiO_3]_{0.31}$ (PMN−PT) single crystal substrate by X-ray microdiffraction and X-ray photoemission electron microscopy, respectively. These two complementary measurements of the same area on the sample indicate the presence of a nonuniform strain which strongly influences the reorientation of the magnetic state within identical Ni microstructures along the surface of the sample. Micromagnetic simulations confirm these experimental observations. This study emphasizes the critical importance of surface and interface engineering on the micron-scale in composite multiferroic structures and introduces a robust method to characterize future devices on these length scales.

KEYWORDS: *Multiferroics, straintronics, magneto-elastic coupling, piezo-strain, electrical magnetization switching*

The goal of controlling the orientation of on-chip magnetic nanostructures with electric fields from patterned electrodes (in contrast to using conventional power hungry external electro-magnets or other current-based approaches[1]) is of broad technological interest for memory,[2−4] logic,[5−7] and even microfluidic[8] applications. To achieve this goal, researchers have intensively studied multiferroic systems composed of either naturally occurring materials with multiple ferroic orders (i.e., ferroelectric and ferromagnetic)[9,10] or composite materials where a heterostructure couples together two separate materials, each possessing a single ferroic order (i.e., a piezoelectric and a ferromagnet).[11−20] The extensively studied heterostructure of a thin ferromagnetic nickel (Ni) film on the piezoelectric substrate $[Pb(Mg_{1/3}Nb_{2/3})O_3]_{1-x}-[PbTiO_3]_x$ (PMN−PT)[8,14,16,21] is one example of a composite multiferroic system. In this system, an applied electric field induces a strain at the piezoelectric/ferromagnet interface. This strain introduces a magneto-elastic energy term that competes with the demagnetization and exchange energies within patterned Ni structures, resulting in the reorientation of their magnetization. Previous measurements of this system have demonstrated an electrically induced, strain-based magnetic reorientation.[8,14,16,18,21−23] Notably, however, identical magnetic structures on a single piezoelectric substrate do not exhibit a

Received: December 19, 2017
Revised: February 20, 2018
Published: February 26, 2018

ACS Publications © 2018 American Chemical Society

DOI: 10.1021/acs.nanolett.7b05342
Nano Lett. 2018, 18, 1952−1961

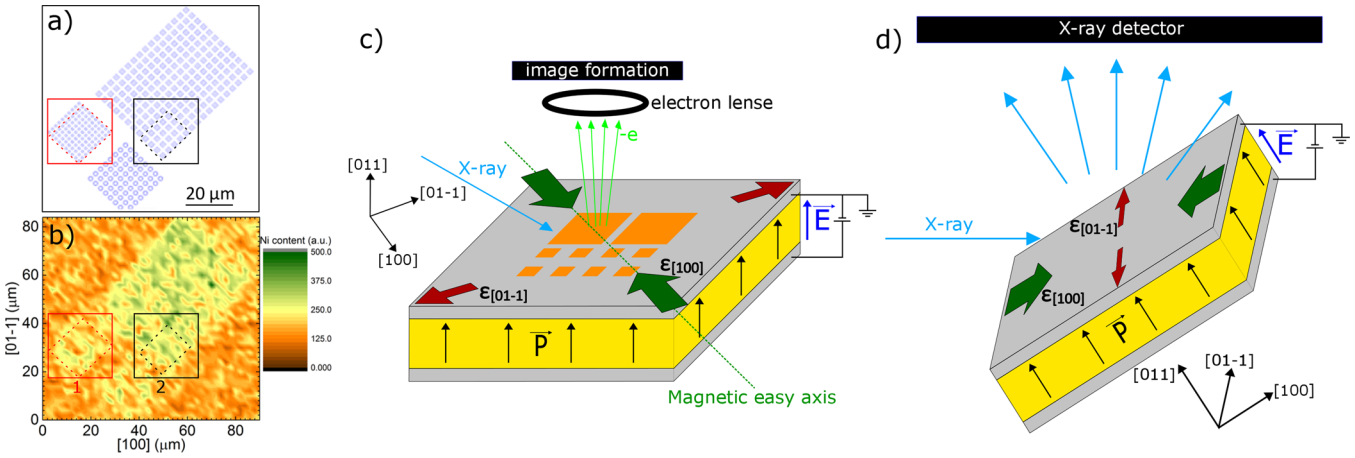

Figure 1. (a) Sample layout: the 1 μm (2 μm) magnetic square array imaged during the XMCD-PEEM experiment is indicated by the dashed red (black) frame. (b) Ni K_α X-ray microfluorescence map of the magnetic microstructures on PMN−PT substrate. Solid red (black) frame indicates Area 1 (Area 2) scanned in the X-ray microdiffraction experiment. (c) Schematic of sample in the XMCD-PEEM experiment. (d) Schematic of the sample in the X-ray microdiffraction experiment (the magnetic structures are omitted from the sample schematic for clarity). In this experiment, the focused X-ray beam was at a 50° angle with respect to the surface normal.

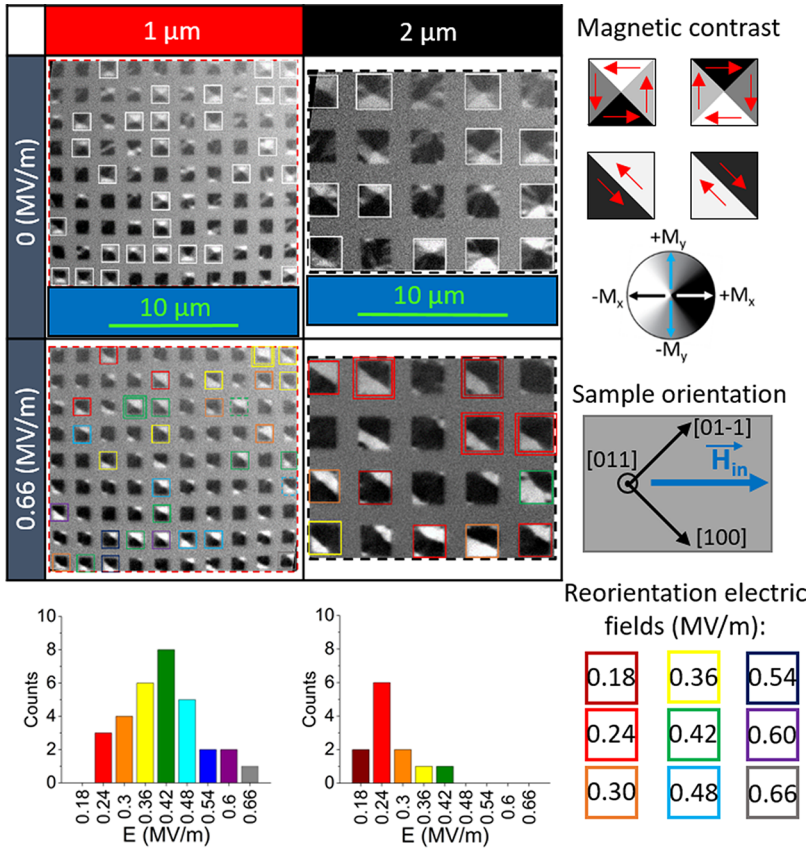

Figure 2. XMCD−PEEM images of 1 and 2 μm Ni squares under the action of an electric field applied through the PMN−PT thickness. White frames indicate the magnetic structures with an initial magnetic vortex state, induced after the application and the subsequent removal of an external magnetic field, $\mu_0 H_{in} \approx 250$ mT. Colored squares indicate the successful electrically driven transformation from a magnetic vortex to a two-domain state. The double frames indicate magnetic squares where a lateral magnetic DW motion is observed. The two bar graphs report the number of reorientation events occurring at each applied electric field for 1 μm (left) and 2 μm (right) squares.

uniform behavior in response to this stimulus. Instead the strain-induced magnetic reorientation within an array of nominally identical structures occurs for a distribution of electric field values or in some cases does not occur at all. Previously, this has been attributed to the presence of ferroelectric domains and domain walls that vary spatially, resulting in a nonuniform strain, on the same micron length scale as the magnetic structures.[8,16] However, to our knowledge no quantitative experimental measurement has yet interrogated the systematic influence of this nonuniform micron-scale strain on magnetic microstructures as a function of the electric field in a composite multiferroic system.

DOI: 10.1021/acs.nanolett.7b05342
Nano Lett. 2018, 18, 1952−1961

In this Letter, we image both the magnetization and strain of a PMN−PT\Ni heterostructure with micrometer-scale resolution, as an applied electric field induces strain in the system. From an analysis of these images, we unveil the connection between the onset of magnetic reorientation and the locally induced piezo-strain. Micron-sized patterned Ni squares are imaged with X-ray magnetic circular dichroism-photoemission electron microscopy (XMCD-PEEM), while the local piezo-strain of the PMN−PT surface in the same area of the Ni squares is mapped by X-ray microdiffraction. Our analysis is further validated by micromagnetic simulations, which correlate well with our experimental observations.

The multiferroic system under investigation consists of a double side polished, 500 μm thick piezoelectric $[Pb(Mg_{1/3}Nb_{2/3})O_3]_{0.69}$−$[PbTiO_3]_{0.31}$ (PMN−PT) single crystal (TRS Technologies, Inc., State College, PA, U.S.A.) with both the top and the bottom surfaces covered by a 50 nm thick Pt electrode. The piezoelectric substrate has the [011]pc (pseudocubic; in the following this index will be omitted for simplicity) crystallographic direction pointing out of the plane of the surface and is electrically prepoled in this direction with the polarization pointing "up" (see Figure 1) before depositing the magnetic Ni layer on top of it. Both 1 and 2 μm large magnetic square arrays, composed of a polycrystalline Ti(5 nm)\Ni(15 nm) bilayer, are patterned on the top of the Pt electrode (see Figure 1) using electron-beam lithography, electron-beam evaporation, and lift-off techniques. Because of the very small thickness to lateral size ratio of the patterned magnetic structures, the strain transferred inside the magnetic layer is expected to be uniform throughout its thickness.

First, we use X-ray magnetic circular dichroism−photoemission electron microscopy (XMCD−PEEM)[24,25] to characterize the onset of an electrically induced magnetic reorientation in an array of Ni squares at room temperature (Figure 1c). A Landau flux-closure state[26] is initially prepared in the magnetic squares, where the magnetization inside the magnetic domains aligns parallel to the edges of the squares. After that, the magnetic moments in the Ni squares are reoriented by an electrically induced strain along the PMN−PT [100] direction. Such magnetic reorientation is driven by the inverse magnetostrictive effect (also known as the magnetoelastic effect or the Villari effect).[27−31] The induced compressive strain generated along PMN−PT[100] imparts a magnetic easy axis 45° from the edges of the squares, as shown in Figure 1c. The resulting easy axis favors a two domain state, where the magnetization in the two domains is aligned along the new magnetic easy axis and in an antiparallel fashion (see micromagnetic results below for more details). The imaged 1 μm (2 μm) large Ni squares are indicated by the dashed red (black) frame in Figure 1a. The magnetic images are taken while the electric field is applied through the sample's thickness.

Prior to imaging, the magnetic microstructures are initialized by a uniform external magnetic field, $\mu_0 H_{in} \approx 250$ mT, parallel to the horizontal edges of the Ni squares (Figure 2). In several of the imaged squares, the desired Landau flux-closure magnetic state (subsequently described as "vortex state") is obtained, as indicated by the white frames in Figure 2. We observe a 32% (60%) yield for the vortex state nucleation in the 1 μm (2 μm) Ni squares in the region of interest. The initialization yield is smaller than 100% because after applying and then removing a uniform magnetic field, two other magnetic configurations are observed. Several devices remain in a single-domain state, which is a local minimum in the magnetostatic energy landscape of the micromagnets. Others are observed in a randomly oriented multidomain state, primarily due to domain wall pinning effects. Indeed, perturbing the system with a small electric field (i.e., a small strain is applied to the magnetic squares) drives some of the noninitialized squares from this local energy minimum to the vortex state global minimum[26] (see Figure S1 in Supporting Information). In this work, we focus on the behavior of the magnetic squares with an initial vortex state.

After initializing the Ni squares into the magnetic vortex state, we apply a direct current (dc) electric field up to 0.66 MV/m in steps of 0.06 MV/m through the thickness of the piezoelectric substrate (i.e., the [011] crystallographic direction, see Figure 1c). While increasing the electric field stepwise, we observe a gradual realignment of the magnetic moments in the Ni microstructures toward the [100] crystallographic direction of the PMN−PT substrate (see Figure S1 in the Supporting Information for more details). At various steps during the ramp, some of the magnetic microsquares are fully strained into a two-domain state with two antiparallel magnetic domains oriented along the PMN−PT [100] axis. At the maximum applied electric field, all of the 1 and 2 μm large Ni squares initially in a vortex-state have reoriented to this configuration. Finally, the electric field is ramped down to 0 MV/m, after which a statistically insignificant number of vortex states remain. The current experimental setup prevents a meaningful reproduction of the experiment. Observing this behavior through multiple cycles will be the subject of future studies.

The electric field values required to reorient the vortex-state in each square spans a range from 0.18 to 0.66 MV/m, as shown in Figure 2. We indicate the electric field amplitude that reorients each square by altering the color of the surrounding frame from white to a color corresponding to the electric field amplitude. The statistical distribution of this reorientation electric field in the imaged areas is described in the two bar graphs at the bottom of Figure 2. The graph on the left (right) reports the count of switched magnetic squares at each applied electric field in the 1 μm (2 μm) square array. A total of 31 (12) 1 μm (2 μm) squares are observed to reorient from a vortex to a two-domain state. For those squares, an average reorientation field of 0.41 MV/m (0.26 MV/m) is extracted for the 1 μm (2 μm) magnetic squares. The larger reorientation field observed for the 1 μm squares, compared to the 2 μm squares, is in agreement with the higher demagnetization energy density generated in the smaller microstructures during the magnetic reorientation. Indeed, this result is reproduced by micromagnetic simulations (see Figure S2 in Supporting Information), where a 1 μm square is found to require a strain (i.e., uniaxial magnetic anisotropy) as large as twice the one needed for the 2 μm square in order to obtain the same degree of magnetic reorientation.

At large applied electric fields, we observe lateral domain wall motion and curving (indicated by double colored frames in Figure 2) in addition to the formation of domains at the corners of some squares. We attribute the lateral domain wall motion and curving to electrically induced strain effects and offer a detailed explanation of this observation later in the manuscript. At this time, we do not fully understand the formation of the corner domains; however, their nucleation at high electric fields suggests a localized minimization of the magnetic energy driven by the presence of a large localized strain. Further modeling of this system may provide a more robust understanding of this mechanism.

DOI: 10.1021/acs.nanolett.7b05342
Nano Lett. 2018, 18, 1952−1961

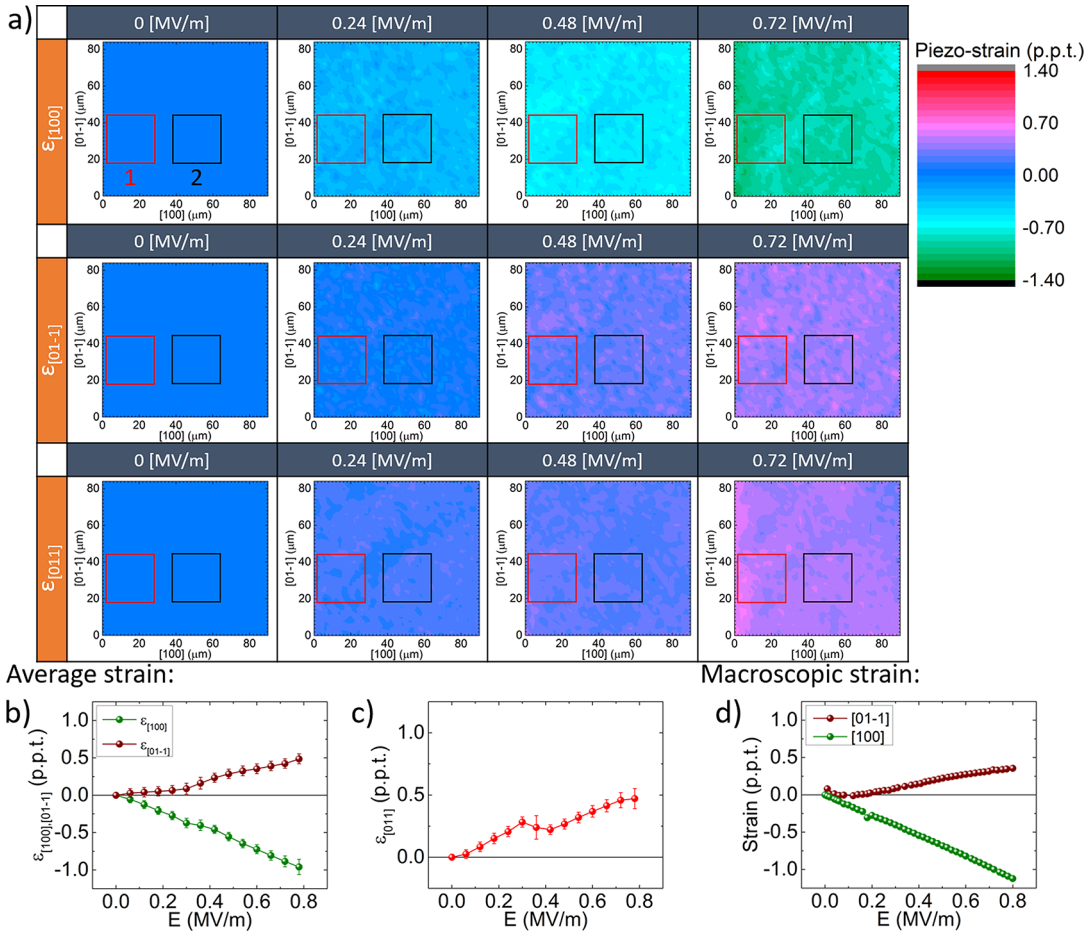

Figure 3. (a) Imaging of the electrically induced piezo-strain at the top surface of the PMN−PT substrate, along its three main crystallographic directions. The imaging pixel size is 2 × 2 μm^2, and the image area corresponds to the one reported in Figure 1a,b. The solid red (black) frame indicates Area 1 (Area 2). (b,c) Average piezo-strain induced along the in-plane and the out-of-plane main crystallographic directions, respectively, as a function of the applied electric field. The error bars indicate the standard deviation of the stain values distribution. (d) The piezo-strain along the two in-plane directions of the substrate measured by a strain gauge is reported for comparison. All strain values are reported in parts per thousand (ppt).

Finally, in Figure 2 we note the presence of localized areas where a number of squares, close to each other, share the same reorientation field, while squares farther apart from each other show a different reorientation field. This is most visible for the 1 μm square case, where a larger number of squares are imaged in the field-of-view. These localized regions with locally shared magnetic behavior, indicate the presence of a global nonuniformity and a spatially varying force driving the magnetic reorientation. Accordingly, we now experimentally examine the electrically induced strain that influences such behavior.

To characterize the micron-scale strain responsible for the distributed onset of magnetic reorientation in the squares, we use Laue (white light) X-ray microdiffraction,[32] as schematically shown in Figure 1d. This allows us to independently measure the electrically induced strain with micron-scale resolution at the location where the XMCD-PEEM measurements were taken. The strain is induced in an identical manner to the XMCD-PEEM measurement, by stepping the electric field from 0.0 to 0.78 MV/m in steps of 0.06 MV/m. A focused 2 μm diameter (full width at half-maximum) X-ray beam is rastered along the sample surface with a step size of 2 μm. A diffraction pattern is captured at each point in the scanned area and compared with the expected one for an ideal unstrained crystal, allowing the extraction of the actual local strain in the sample.[33] By subtracting the extracted strain at zero electric field from the one in the presence of a finite electric field, we calculate the electrically induced piezo-strain as a function of the applied field, pixel by pixel. Finally, the extracted piezo-strain is presented as a two-dimensional (2D) map, as shown in Figure 3a.

The sample is scanned along the [100] and the [01$\bar{1}$] crystallographic directions of the substrate, which are known to be the in-plane directions along which compressive (ε < 0) and tensile (ε > 0) strains, respectively, are induced when an electric field is applied along the [011] direction.[8,17,19] The electrically induced piezo-strains along the three main crystallographic directions, $\varepsilon_{[100]}$, $\varepsilon_{[01\bar{1}]}$, and $\varepsilon_{[011]}$ are measured in the area shown in Figure 1b, which contains the imaged magnetic arrays. The obtained strain maps are shown in Figure 3a (the complete data are reported in Figure S3 of the Supporting Information).

First, we observe that an average compressive strain is electrically induced along the [100] direction, while tensile strain is induced along the [01$\bar{1}$] and the [011] directions. This is more clearly shown in the graphs in Figure 3b,c where the average strain values in the imaged 90 × 84 μm^2 large area are plotted as a function of the applied electric field for the in-plane and out-of-plane directions, respectively. We complement this

DOI: 10.1021/acs.nanolett.7b05342
Nano Lett. 2018, 18, 1952−1961

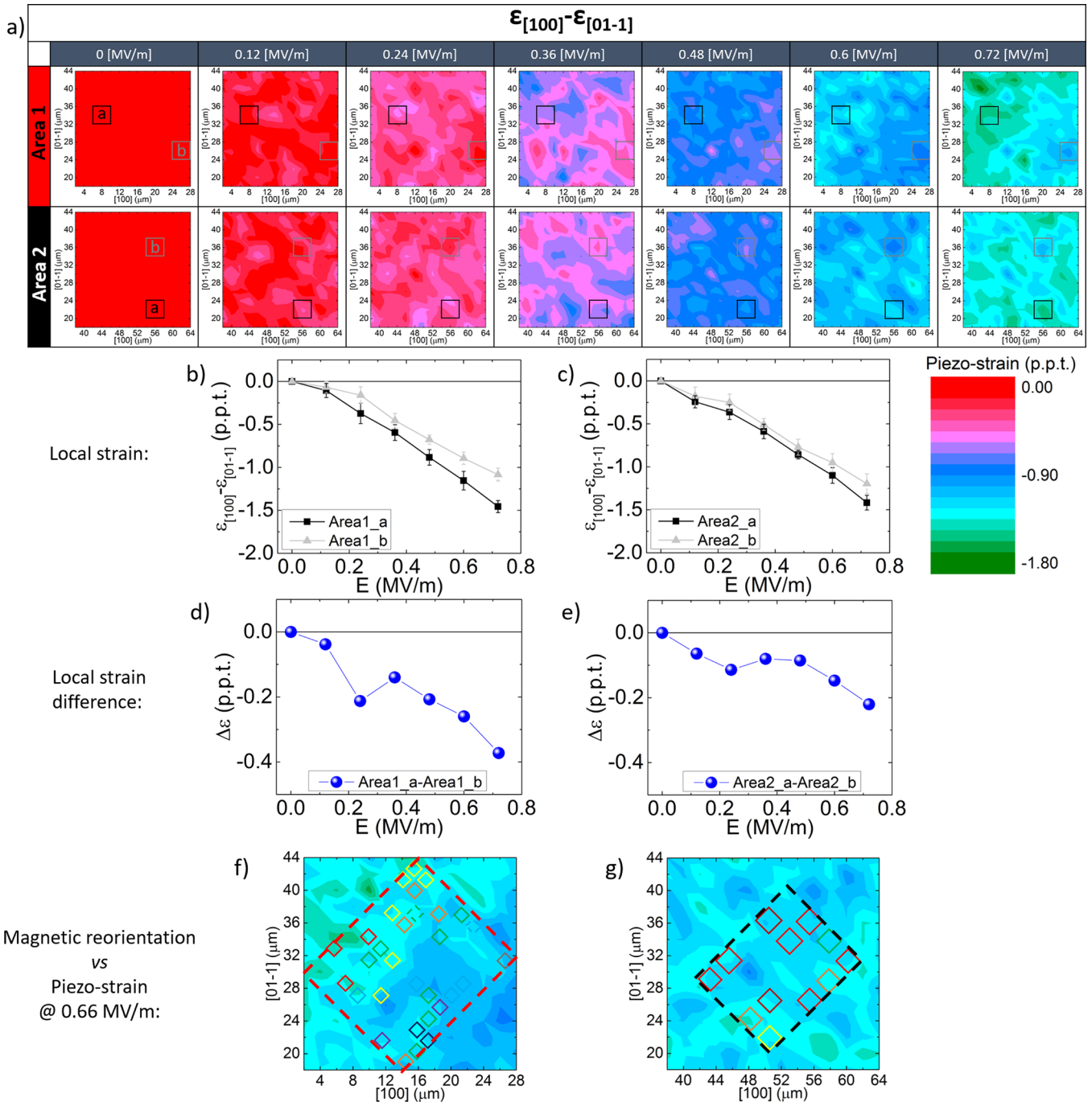

Figure 4. (a) Imaging of the in-plane piezo-strain, $\varepsilon_{[100]} - \varepsilon_{[01\bar{1}]}$, at the location of the 1 μm (Area 1) and 2 μm (Area 2) square arrays. Two local 4 × 4 μm^2 regions, *a* (large strain, black frame) and *b* (small strain, gray frame), are chosen in both Area 1 and Area 2. (b,c) The average strain induced locally in regions *a* (black squares) and *b* (gray triangles), as a function of the electric field. (d,e) The electric-field dependence of the difference between the average strain in region *a* and in region *b* for Area 1 and Area 2, respectively. (f,g) Comparison between the magnetic reorientation observed by XMCD−PEEM and reported in Figure 2 (the colored frames indicate the reorienting electric field) and the imaged piezo-electric state at E = 0.66 MV/m in Area 1 and Area 2, respectively. All strain values are reported in ppt.

data by also measuring the response from a strain gauge fixed on top of the sample, shown in Figure 3d, where the measured electric field dependence of the piezo-strain along [100] and $[01\bar{1}]$ is plotted in green and dark red, respectively. Comparing the data in Figure 3b,d, we conclude that averaging the strain response within the 90 × 84 μm^2 raster window adequately captures the macroscopic piezoelectric behavior of the PMN−PT substrate.

Second, the images in Figure 3a report the presence of a nonhomogenous piezo-strain within the investigated area, as also indicated by the finite error bars in the graphs in Figure 3b,c. In those images, a nonuniform strain pattern is visible, where regions with larger magnitude strain values are separated by regions with smaller strain values.

In order to obtain a more direct comparison between the observed electrically induced magnetic reorientation and the piezo-strain measured at the micrometer scale, the strain maps

DOI: 10.1021/acs.nanolett.7b05342
Nano Lett. 2018, 18, 1952−1961

for Area 1 (red solid frame) and Area 2 (black solid frame) shown in Figure 3a are reported in Figure 4a. The displayed color maps report the total in-plane piezo-strain, $\varepsilon_{[100]} - \varepsilon_{[01\bar{1}]}$, because this is the actual driving force to the observed magneto-elastic effect[16,21] reported in Figure 2. For both Area 1 and Area 2, the strength of the measured piezo-strain is spatially nonuniform. In Figure 4a, the strain pattern is clearly visible showing that "large strain" and "small strain" regions are both present in the imaged areas (which are, respectively, the green and the blue regions, at the maximum applied electric field).

It is worth noting that Area 1 and Area 2 are defined based on the X-ray microfluorescence map at the Ni edge reported in Figure 1b, which is obtained by scanning the focused X-ray beam on the sample surface with a 2 μm step-size. The definition of these two areas in the strain maps, which is an attempt to localize the position of the imaged magnetic squares (dashed frames inside Area 1 and Area 2), is affected by an error of the order of the convolution of the step size with the X-ray beam size (~3 μm), which is of the same order as the square dimensions. Thus, a direct visual correlation at the single magnetic square-level is not allowed by the resolution of our measurements. However, a meaningful analysis of the visual correlation between the reorientation fields and the strain maps can be performed within the resolution limit on regions like the XMCD−PEEM viewing area with dimensions on the order of tens of microns.

From the microdiffraction data, we quantify the local strain dependence as a function of the applied electric field at two different locations within Area 1 and Area 2. One large strain region, *a* (black frame), and one small strain region, *b* (gray frame), both 4 × 4 μm^2 in size, are chosen in Figure 4a for this analysis. In Figure 4b,c, it can be seen that the average total piezo-strain, $\varepsilon_{[100]} - \varepsilon_{[01\bar{1}]}$, in region *a* (black squares) is always larger than in region *b* (gray triangles), for all of the applied electric field magnitudes. This is more directly shown in Figure 4d,e, where the electric field dependence of the difference between the strain in *a* and in *b* is shown, respectively, for Area 1 and Area 2. The local strain differences are observed to increase with increasing electric field with a maximum value of $\Delta\varepsilon$ = 0.37 ppt measured at the maximum applied electric field.

By using a phenomenological model to describe the magneto-elastic effect induced in this composite multiferroic system, the electrically controlled strain-induced magneto-elastic uniaxial anisotropy energy density can be evaluated using the following equation[34]

$$U_{\mathrm{me}} = \frac{3}{2}\lambda_{\mathrm{p}} Y(\varepsilon_{[100]} - \varepsilon_{[01\bar{1}]})\sin^2\theta_{[100]} \quad (1)$$

where λ_{p} is the saturation magnetostriction constant for polycrystalline Ni, Y is the Young's modulus for Ni, and $\theta_{[100]}$ is the angle between the magnetization direction and the compressive strain direction of the piezoelectric, [100]. From eq 1, it is possible to define a magneto-elastic uniaxial anisotropy factor: $K_{\mathrm{me}} = \frac{3}{2}\lambda_{\mathrm{p}} Y(\varepsilon_{[100]} - \varepsilon_{[01\bar{1}]})$, which is a function of the electrically induced piezo-strain.

It is now possible to translate the experimentally measured local strain values into the equivalent local magneto-elastic anisotropy energy density, which is the actual driving force in the observed electrically induced magnetic reorientation. A nonuniform strain distribution corresponds to a nonuniform U_{me} in the magnetic arrays, which is expected to result in a nonuniform activation of the different magnetic squares.

In order to quantify the influence of the nonuniformity of the strain on the magnetic reorientation effect, we compare the locally induced magnetoelastic anisotropy energy densities between the small strain and the large strain regions. The measured strain values at the selected small strain regions (*b* regions) for the average reorientation fields are ε_{A1_b} = −0.55 ppt (at E = 0.42 MV/m) for the 1 μm squares and ε_{A2_b} = −0.25 ppt (at E = 0.24 MV/m) for the 2 μm squares. On the basis of eq 1, these strain values correspond to[35] K_{A1_b} = −10.5 kJ/m^3 and K_{A2_b} = 5.7 kJ/m^3. Furthermore, the strain differences between region *a* and region *b* at the same electric fields correspond to the following differences in the induced uniaxial magnetic anisotropy: ΔK_{A1_b} = 3.9 kJ/m^3 and ΔK_{A2_b} = 2.5 kJ/m^3. On the basis of this, we can calculate a relative magnetic anisotropy energy difference of $\Delta K/K_b$ = 0.37 and 0.44 for Area 1 and Area 2, respectively. As a result, during the reorientation process the difference in the locally induced K_{me} between two different magnetic squares, one sitting on top of a small strain region and one on top of a large strain region, just a few microns apart, can be as large as 37% and 44% in the two studied areas.

We experimentally verify the analysis above in Figure 4f,g, where we overlay the electric field activation data shown in Figure 2 on top of a strain maps taken at 0.66 MV/m for both the 1 and 2 μm squares, respectively, to directly compare the reorientation field distribution (colored frames) and the local strain configuration. The microdiffraction data for E = 0.66 MV/m presented in Figure 4f indicates the presence of a significant strain inhomogeneity within the XMCD−PEEM viewing area (dashed red frame) which drastically influences the magnetic reorientation behavior of the 1 μm squares. We analyze this data assuming the Ni squares are nominally identical across the entire viewing area. The squares located in the blue strain region (approximately from −0.90 to −1.2 ppt at 0.66 MV/m) tend to remain in the vortex state longer and require a stronger electric field (green−blue−violet frames) to generate enough strain to drive magnetic reorientation. On the other hand, the squares located in the green strain regions (from −1.2 to −1.5 ppt at 0.66 MV/m) tend to reorient at lower electric fields (red−orange−yellow frames), correlating well with the larger local strain present in that region of the sample. This observation agrees with our analysis of the strain data above, where we concluded that closely spaced, nominally identical magnetic squares subject to widely varying local strains experience significantly distinct local magnetoelastic anisotropies. These local magnetoelastic anisotropies drive the spatial distribution of the strain-dependent magnetic reorientation in the squares. Furthermore, the microdiffraction data with the overlaid 2 μm squares reorientation behavior presented in Figure 4g compliments this result. In this case, the XMCD−PEEM viewing area (dashed black frame) is subject to more homogeneous local strains (approximately −1.2 ppt at 0.66 MV/m), resulting in a tighter distribution of the electric field required to induce magnetic reorientation, driven by more similar local magnetoelastic anisotropies.

It is worth noting that, while the reorientation of the squares is driven by the local magnetoelastic anisotropies, pinning due to interface inhomogeneities or fabrication defects may also contribute to the distribution of reorientation fields observed in Figure 2. Our analysis of the data, however, suggests these effects are minimal. We observe a continuous and deterministic magnetic rotation within the structures befitting of the strain-based control rather than the discontinuous propagation of

DOI: 10.1021/acs.nanolett.7b05342
Nano Lett. 2018, 18, 1952−1961

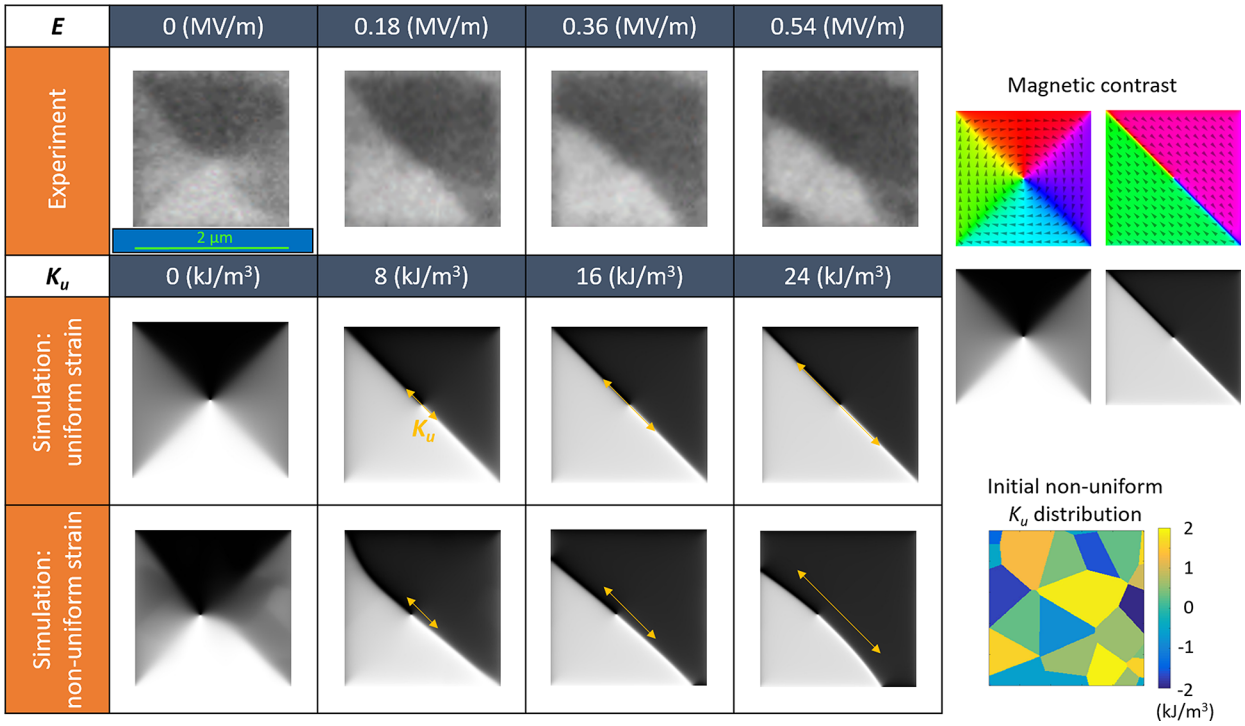

Figure 5. Comparison between the strain-induced activation of a 2 μm magnetic square observed experimentally and the outcome of micromagnetic simulations. The first row reports the magnetic state of one of the magnetic squares observed by XMCD−PEEM, as a function of the applied electric field. The second and third rows report the outcome of micromagnetic simulations where an increasing uniform and nonuniform magnetic uniaxial anisotropy, K_u, is applied, respectively. The color map at the bottom-right shows the random polygon map used for defining the initial nonuniform K_u distribution present in the latter micromagnetic simulation.

domain walls moving through pinning sites along the edges of the structures. This is particularly true for the 2 μm squares. Furthermore, a small edge roughness is confirmed by scanning electron microscopy imaging (see Figure S4 in Supporting Information). Interestingly, a recent study[36] has shown that interface defects introduced by the PMN−PT surface roughness can be reduced by depositing a thin film polymer between the PMN−PT and Pt layers, offering a possible path toward a pinning-free multiferroic system with a more uniform magnetic response.

On the basis of our findings, we thus conclude that the observed nonuniform electrical activation of magnetic squares reported in Figure 2 is due to the nonuniform spatial distribution of the piezo-strain induced at the PMN−PT substrate top surface (as shown in Figure 4), which results in a nonuniform magneto-elastic anisotropy acting on the magnetic structures.

To further understand the electrical activation of magnetic squares reported above, micromagnetic simulations are carried out using a MuMax code[37,38] (see Section S2 in the Supporting Information). Here we focus on understanding how the magnetic reorientation process presented above would be affected by the presence of a nonuniform strain inside a single magnetic square.

A 2 μm × 2 μm magnetic Ni square is simulated, where a Landau initial state is modified by a stepwise increase of a uniaxial anisotropy energy term (which, according to the phenomenological model presented above, corresponds to the application of a uniaxial strain). Two different simulations are carried out; the first one assumes a uniform strain (i.e., a uniform uniaxial magnetic anisotropy); the second one includes the presence of a nonuniform strain. In both cases, the uniaxial strain is oriented along one of the square's diagonals, so as to reproduce the same conditions of the actual experiment. More details can be found in Section S2 of the Supporting Information.

In Figure 5, the outcome of the micromagnetic simulations is compared with the experimental data for one of the 2 μm × 2 μm magnetic Ni squares reported in Figure 2. The experimental results are reported in the first row of Figure 5, while the outcome of the micromagnetic simulations with uniform strain and nonuniform strain are reported in the second and third row, respectively. The four images of the experimental Ni square show the observed magnetic steady state when an electric field of 0, 0.18, 0.36, and 0.54 MV/m is applied through the PMN−PT substrate. On the other hand, the frames shown for the simulations are chosen in the following way. For the uniform strain case, the first image is the steady state obtained with zero initial strain, that is, no uniaxial magnetic anisotropy. For the nonuniform strain case, the first image is the initial steady state considering the nonzero initial magnetic anisotropy (see color map at the bottom right of Figure 5). Such an initial magnetic anisotropy configuration is defined by randomly generating a polygon map and subsequently randomly assigning a value for the anisotropy energy density to each of the polygons. The range of values (from −2 kJ/m^3 to +2 kJ/m^3) is chosen based on the values of strains reported in Figure 4e, so as to replicate the strain nonuniformity present in the experimental system (see Supplementary Section S2 for more details). The other frames correspond to the application of a uniform uniaxial anisotropy energy density, $E_u = K_u \sin^2(\theta_{[100]})$, with K_u values of 8, 16, and 24 kJ/m^3, which is added to the initial anisotropy defined in the magnetic square (zero for the uniform case, nonzero for the nonuniform case). By equating

DOI: 10.1021/acs.nanolett.7b05342
Nano Lett. 2018, 18, 1952−1961

K_u and K_{em}, and assuming a linearly increasing piezo-strain at a rate of 0.35 (ppt)/0.18 (MV/m) (based on the data reported in Figure 4e for region *a*), the experimental observations are quantitatively reproduced by the micromagnetic simulation for the following parameters: $\lambda_p = -69 \times 10^{-6}$ and $Y = 220$ GPa. The latter is the bulk Young's modulus of polycrystalline Ni, while $\lambda_p = -69 \times 10^{-6}$ is close to the range of experimentally reported values of the saturation magnetostriction constant for polycrystalline Ni.[35]

Experimentally, as the electric field is increased stepwise, the magnetic state inside the Ni square is observed at first to transform from an initial Landau flux-closure state to a two-domain state. Subsequently, for even larger electric field values the magnetic domain wall (DW) separating the two domains is observed to curve and propagate toward the bottom left corner of the square. When compared to the results of the micromagnetic simulations, both cases reproduce the vortex to two-domain transformation but only the simulation with a nonuniform strain is able to reproduce the curving and the lateral motion of the magnetic DW.

The interpretation of the observed magnetic DW motion is then the following. The nonuniformity of the strain inside the square results in a spatially varying magnetic energy landscape, which evolves as the electric field is increased. As the electric field increases, spatial differences in strain intensify and eventually induce a DW motion from strain regions with larger anisotropy (K) to strain regions with smaller anisotropy. Accordingly, the DW motion is driven by the minimization of its energy density, $\sigma_{DW} \propto \sqrt{A_{ex}K}$, where A_{ex} is the micromagnetic exchange constant and K is the total magnetic anisotropy. Furthermore, the propagation of the DW away from the diagonal of the square is assisted by the shortening of the DW which further decreases the total DW energy, $\epsilon_{DW} \propto \sigma_{DW} l_{DW}$; where l_{DW} is the length of the magnetic DW. Finally, the dipolar field energy, which increases while the system evolves away from the perfectly symmetric two-domain state, counteracts the DW motion in order to minimize itself. All this results in a stepwise motion of the DW, which propagates at each increase of the strain as a result of the balance between the lowering of the DW energy and the increase of the dipolar energy.

This finding is further confirmation that the magnetic squares in the multiferroic actuator are experiencing a nonuniform strain. The strain can be nonuniform, not only from square to square, as revealed by our X-ray microdiffraction experiments, but also within the same square, substantially affecting the ideal behavior of the multiferroic system.

In summary, we have performed a systematic, micron-scale study of the physical mechanisms which drive a PMN−PT/Ni multiferroic actuator. We correlated the electric-field distribution required to drive magnetic reorientations in micron-scale Ni squares to the micron-scale local strain environment, by separately measuring the strain (by X-ray microdiffraction) and magnetic response (by XMCD−PEEM) to an applied electric field at the same location in the multiferroic device. With an electric field applied uniformly over the surface, areas separated by microns were observed with distinctly different strain amplitudes driving significant local spatial variations of the magnetoelastic anisotropy. As the electric field was increased, this distribution of nonuniform strains drove the nominally identical magnetic squares to reorient over a range of electric fields. This experimentally observed behavior was verified with a micromagnetic model. Our systematic study emphasizes the importance of the interface in composite multiferroic structures. Surface and interface engineering at the micron-scale is critical to achieve uniform magnetic responses to electrically induced strains even on polished, prepoled, single-crystal substrates.[36] This fusion of experimental techniques (XMCD−PEEM and X-ray microdiffraction) enables robust assessments of future composite multiferroic devices at these length scales.

■ ASSOCIATED CONTENT

Supporting Information

The Supporting Information is available free of charge on the ACS Publications website at DOI: 10.1021/acs.nanolett.7b05342.

XMCD-PEEM imaging of the electrical activation of Ni squares; the direct characterization of the piezo-strain at the top surface of the PMN-PT substrate; the micromagnetic model used for carrying out the micromagnetic simulations; the structural characterization of the magnetic Ni microstructures (PDF)

■ AUTHOR INFORMATION

Corresponding Authors

*E-mail: rloconte@berkeley.edu (R.L.C.).
*E-mail: jbokor@berkeley.edu (J.B.).

ORCID

Roberto Lo Conte: 0000-0002-5050-9978
Camelia V. Stan: 0000-0002-5025-5568

Author Contributions

R.L.C. wrote the manuscript; R.L.C. and C.C. prepared the Supporting Information. Z.X. prepared the sample. R.L.C., Z.X., and A.S. carried out the XMCD-PEEM imaging experiment; R.L.C. and Z.X. carried out the data analysis. R.L.C., Z.X., C.V.S., J.G., A.E.-G., and N.T. carried out the X-ray microdiffraction experiment; R.L.C., C.V.S., A.P., and Z.X. carried out the data analysis. C.C. carried out the micromagnetic simulations. R.L.C., M.E.N., and J.B. designed the experiments. All authors discussed the results and contributed to the preparation of the manuscript. All authors have given approval to the final version of the manuscript.

Notes

The authors declare no competing financial interest.

■ ACKNOWLEDGMENTS

We gratefully acknowledge support from the National Science Foundation (NSF) through the Cooperative Agreement Award EEC-1160504 for Solicitation NSF 11-537 (TANMS) and the NSF Center for Energy Efficient Electronics Science. The work at the Advanced Light Source at Lawrence Berkeley National Laboratory (XMCD-PEEM at beamline 11.0.1 and X-ray microdiffraction at beamline 12.3.2) is supported by the Director, Office of Science, Office of Basic Energy Sciences, U.S. Department of Energy, under contract number DE-AC02-05CH11231. This work was also supported by the Director, Office of Science, Office of Basic Energy Sciences, Materials Sciences and Engineering Division, of the U.S. Department of Energy under Contract No. DE-AC02-05-CH11231 within the Nonequilibrium Magnetic Materials Program (MSMAG). We also acknowledge the use of the fabrication facility at the Integrated Systems Nanofabrication Cleanroom of the

DOI: 10.1021/acs.nanolett.7b05342
Nano Lett. 2018, 18, 1952−1961

California NanoSystems Institute. Finally, we are thankful to Juan Pablo Llinas from the University of California in Berkeley for his support in the SEM imaging of our sample.

REFERENCES

(1) Wang, K. L.; Alzate, J. G.; Khalili Amiri, P. Low-power non-volatile spintronic memory: STT-RAM and beyond. *J. Phys. D: Appl. Phys.* **2013**, *46*, 074003.
(2) Novosad, V.; Otani, Y.; Ohsawa, A.; Kim, S. G.; Fukamichi, K.; Kioke, J.; Maruyama, K.; Kitakami, O.; Shimada, Y. Novel magneto-strictive memory device. *J. Appl. Phys.* **2000**, *87*, 6400.
(3) Bibes, M.; Barthélémy, A. Towards a magnetoelectric memory. *Nat. Mater.* **2008**, *7*, 425−426.
(4) Wang, Q.; Li, X.; Liang, C.-Y.; Barra, A.; Domann, J.; Lynch, C.; Sepulveda, A.; Carman, G. Strain-mediated 180° switching in CoFeB and Terfenol-D nanodots with perpendicular magnetic anisotropy. *Appl. Phys. Lett.* **2017**, *110*, 102903.
(5) Salehi Fashami, M.; Atulasimha, J.; Bandyopadhyay, S. Magnetization dynamics, throughput and energy dissipation in a universal multiferroic nanomagnetic logic gate with fan-in and fan-out. *Nanotechnology* **2012**, *23*, 105201.
(6) Lei, N.; Devolder, T.; Agnus, G.; Aubert, P.; Daniel, L.; Kim, J.-V.; Zhao, W.; Trypiniotis, T.; Cowburn, R. P.; Chappert, C.; Ravelosona, D.; Lecoeur, P. Strain-controlled magnetic domain wall propagation in hybrid piezoelectric/ferromagnetic structures. *Nat. Commun.* **2013**, *4*, 1378.
(7) Manipatruni, S.; Nikonov, D. E.; Ramesh, R.; Li, H.; Young, I. A. Spin-Orbit Logic with Magnetoelectric Switching: A Multi-Generation Scalable Charge Mediated Nonvolatile Spintronic Logic. 2017, arXiv:1512.05428v2.
(8) Sohn, H.; Nowakowski, M. E.; Liang, C.-Y.; Hockel, J. L.; Wetzlar, K.; Keller, S.; McLellan, B. M.; Marcus, M. A.; Doran, A.; Young, A.; Kläui, M.; Carman, G. P.; Bokor, J.; Candler, R. N. Electrically Dirven Magnetic Domain Wall Rotation in Multiferroic Heterostructures to Manipulate Suspended On-Chip Magnetic Particles. *ACS Nano* **2015**, *9*, 4814−4826.
(9) Eerenstein, W.; Mathur, N. D.; Scott, J. F. Multiferroic and magnetoelectric materials. *Nature* **2006**, *442*, 759−765.
(10) Ramesh, R.; Spaldin, A. N. Multiferroics: progress and prospects in thin films. *Nat. Mater.* **2007**, *6*, 21−29.
(11) Liu, G.; Nan, C.-W.; Cai, N.; Lin, Y. Dependence of giant magnetoelectric effect on interfacial bonding for multiferroic laminated composites of rare-earth-iron alloys and lead-zirconate-titanate. *J. Appl. Phys.* **2004**, *95*, 2660.
(12) Wu, T.; Bur, A.; Zhao, P.; Mohanchandra, K. P.; Wong, K.; Wang, K. L.; Lynch, C. S.; Carman, G. P. Giant electric-field-induced reversible and permanent magnetization reorientation on magneto-electric Ni/(011) $[Pb(Mg_{1/3}Nb_{2/3})O_3]_{(1-x)}$-$[PbTiO_3]_x$ heterostructure. *Appl. Phys. Lett.* **2011**, *98*, 012504.
(13) Lahtinen, T. H. E.; Franke, K. J. A.; van Dijken, S. Electric-field control of magnetic domain wall motion and local magnetization reversal. *Sci. Rep.* **2012**, *2*, 258.
(14) Hockel, J. L.; Bur, A.; Wu, T.; Wetzlar, K. P.; Carman, G. P. Electrically controlled reversible and hysteretic magnetic domain evolution in nickel film/$[Pb(Mg_{1/3}Nb_{2/3})O_3]_{0.68}$-$[PbTiO_3]_{0.32}$ (011) heterostructure. *Appl. Phys. Lett.* **2012**, *100*, 022401.
(15) Liu, M.; Hoffman, J.; Wang, J.; Zhang, J.; Nelson-Cheeseman, B.; Bhattacharya, A. Non-volatile ferroelastic switching of the Verwey transition and resistivity of epitaxial Fe_3O_4/PMN-PT (011). *Sci. Rep.* **2013**, *3*, 1878.
(16) Buzzi, M.; Chopdekar, R. V.; Hockel, J. L.; Bur, A.; Wu, T.; Pilet, N.; Warnicke, P.; Carman, G. P.; Heyderman, L. J.; Nolting, F. Single Domain Spin Manipulation by Electric Field in Strain Coupled Artificial Multiferroic Nanostructures. *Phys. Rev. Lett.* **2013**, *111*, 027204.
(17) Zhang, S.; Zhao, Y.; Xiao, X.; Wu, Y.; Rizwan, S.; Yang, L.; Li, P.; Wang, J.; Zhu, M.; Zhang, H.; Jin, X.; Han, X. Giant electrical modiulation of magnetization in $Co_{40}Fe_{40}B_{20}$/Pb-$(Mg_{1/3}Nb_{2/3})_{0.7}Ti_{0.3}O_3$(011) heterostructure. *Sci. Rep.* **2015**, *4*, 3727.
(18) Ahmad, H.; Atulasimha, J.; Bandyopadhyay, S. Reversible strain-induced magnetization switching in FeGa nanomagnets: Pathway to a rewritable, non-volatile, non-toggle, extremely low-energy straintronic memory. *Sci. Rep.* **2016**, *5*, 18264.
(19) Heidler, J.; Piamonteze, C.; Chopdekar, R. V.; Uribe-Laverde, M. A.; Alberca, A.; Buzzi, M.; Uldry, A.; Delley, B.; Bernhard, C.; Noltig, F. Manipulating magnetism in $La_{0.7}Sr_{0.3}MnO_3$ via piezostrain. *Phys. Rev. B: Condens. Matter Mater. Phys.* **2015**, *91*, 024406.
(20) Hu, J. M.; Chen, L.-Q.; Nan, C.-W. Multiferroic Heterostructures Integrating Ferroelectric and Magnetic Materials. *Adv. Mater.* **2016**, *28*, 15−39.
(21) Finizio, S.; Foerster, M.; Buzzi, M.; Krüger, B.; Jourdan, M.; Vaz, C. A. F.; Hockel, J.; Miyawaki, T.; Tkach, A.; Valencia, S.; Kronast, F.; Carman, G. P.; Noltig, F.; Kläui, M. Magnetic Anisotropy Engineering in Thin Film Ni Nanostructures by Magnetoelastic Coupling. *Phys. Rev. Appl.* **2014**, *1*, 021001.
(22) Cui, J.; Liang, C. Y.; Paisley, E. A.; Sepulveda, A.; Ihlefeld, J. F.; Carman, G. P.; Lynch, C. S. Generation of localized strain in a thin film piezoelectric to control individual magnetoelectric heterostructuires. *Appl. Phys. Lett.* **2015**, *107* (9), 092903.
(23) Foerster, M.; Macià, F.; Statuto, N.; Finizio, S.; Hernández-Mínguez, A.; Lendínez, S.; Santos, P. V.; Fontcuberta, J.; Hernàndez, J. M.; Kläui, M.; Aballe, L. Direct imaging of delayed magneto-dyanmic modes induced by surface acoustic waves. *Nat. Commun.* **2017**, *8* (1), 407.
(24) Scholl, A. Thin-Film Magnetism: PEEM Studies. *Encyclopedia of Materials: Science and Technology*, second ed.; ELSEVIER Science Ltd., 2002; pp 1−5. https://doi.org/10.1016/B0-08-043152-6/01823-4.
(25) Chen, C. T.; Sette, F.; Ma, Y.; Modesti, S. Soft x-ray magnetic circular dichroism at the $L_{2,3}$ edges of Nickel. *Phys. Rev. B: Condens. Matter Mater. Phys.* **1990**, *42*, 7262−7265.
(26) Hubert, A.; Schäfer, R. *Magnetic Domains: The Analysis of Magnetic Microstructures*; Springer-Verlag: Berlin,1998.
(27) Lee, E. W. Magnetostriction and Magnetomechanical Effects. *Rep. Prog. Phys.* **1955**, *18*, 184−229.
(28) Furthmüller, J.; Fähnle, M.; Herzer, G. Theory of magneto-striction in amorphous and polycrystalline ferromagnets: I. Description of the Formalism. *J. Magn. Magn. Mater.* **1987**, *69*, 79−88.
(29) Bichurin, M. I.; Petrov, V. M.; Srinivasan, G. Theory of low-frequency magnetoelectric coupling in magnetostrictive-piezoelectric bilayers. *Phys. Rev. B: Condens. Matter Mater. Phys.* **2003**, *68*, 054402.
(30) Salach, J.; Szewczyk, R.; Bieńkowski, A.; Frydrych, P. Methodology of testing the magnetoelastic characteristics of ring-shapes cores under uniform compressive and tensile stresses. *J. Electr. Eng.* **2010**, *61*, 93−95.
(31) Dapino, M. J.; Smith, R. C.; Calkins, F. T.; Flatau, A. B. A Coupled Magnetomechanical Model for Magnetostrictive Transducers and its Application to Villari-Effect Sensors. *J. Intell. Mater. Syst. Struct.* **2002**, *13*, 737−747.
(32) Kunz, M.; Tamura, N.; Chen, K.; MacDowell, A. A.; Celestre, R. S.; Church, M. M.; Fakra, S.; Domning, E. E.; Glossinger, J. M.; Kirschman, J. L.; Morrison, G. Y.; Plate, D. W.; Smith, B. V.; Warwick, T.; Yashchuk, V. V.; Padmore, H. A.; Ustundag, E. A dedicated superbend x-ray microdiffraction beamline for materials, geo-, and environmental sciences at the advanced light source. *Rev. Sci. Instrum.* **2009**, *80*, 035108.
(33) Tamura, N. *Microdiffraction analysis: Strain and dislocation gradients from diffraction: Spatially Resolved Local Structure and Defects*; Imperial College Press: London, 2014; pp 125−155.
(34) Cullity, B. D.; Graham, C. D. *Introduction to Magnetic Materials*, second ed.; John Wiley & Sons, Inc., Publication, 2009.
(35) The following values have been used for the parameters in eq 1 in order to quantify the magneto-elastic anisotropy energy density generated in our system: $\lambda_p = -69*10^{-6}$; Y = 220 GPa. This value of Y is the bulk value for Ni, while the chosen λ_p is close to the values reported in literature for polycrystalline Ni (see ref 34, and Ledbetter,

DOI: 10.1021/acs.nanolett.7b05342
Nano Lett. 2018, 18, 1952−1961

H. M.; Reed, R. P. Elastic Properties of Metals and Alloys, I. Iron, Nickel and Iron-Nickel Alloys. *J. Phys. Chem. Ref. Data* **1973**, *2*, 531.
(36) Xiao, Z.; Mohanchandra, K. P.; Lo Conte, R.; Karaba, C. T.; Schneider, J. D.; Chavez, A.; Tiwari, S.; Sohn, H.; Nowakowski, M. E.; Scholl, A.; Tolbert, S. H.; Bokor, J.; Carman, G. P.; Candler, R. N. Enhanced magnetoelectric coupling in a composite multiferroic system via interposing a thin film polymer. *AIP Adv.* **2018**, *8*, 055907.
(37) Vansteenkiste, A.; Leliaert, J.; Dvornik, M.; Helsen, M.; Garcia-Sanchez, F.; Van Waeyenberge, B. The design and verification of MuMax3. *AIP Adv.* **2014**, *4* (10), 107133.
(38) Navabi, A.; Chen, C.; Barra, A.; Yazdani, M.; Yu, G.; Montazeri, M.; Aldosary, M.; Li, J.; Wong, K.; Hu, Q.; Shi, J.; Carman, G. P.; Sepulveda, A. E.; Amiri, P. K.; Wang, K. L. Efficient Excitation of High-Frequency Exchange-Dominated Spin Waves in Periodic Ferromagnetic Structures. *Phys. Rev. Appl.* **2017**, *7*, 034027.

DOI: 10.1021/acs.nanolett.7b05342
Nano Lett. 2018, 18, 1952−1961